The Company of Biologists

RESEARCH ARTICLE

The β8 integrin cytoplasmic domain activates extracellular matrix adhesion to promote brain neurovascular development

Arpan De, John E. Morales, Zhihua Chen, Sumod Sebastian and Joseph H. McCarty*

ABSTRACT

In the developing mammalian brain, neuroepithelial cells interact with blood vessels to regulate angiogenesis, blood-brain barrier maturation and other key neurovascular functions. Genetic studies in mice have shown that neurovascular development is controlled, in part, by *Itgb8*, which encodes the neuroepithelial cell-expressed integrin β8 subunit. However, these studies have involved complete loss-of-function *Itgb8* mutations, and have not discerned the relative roles for the β8 integrin extracellular matrix (ECM) binding region versus the intracellular signaling tail. Here, Cre/lox strategies have been employed to selectively delete the cytoplasmic tail of murine Itgb8 without perturbing its transmembrane and extracellular domains. We report that the β8 integrin cytoplasmic domain is essential for inside-out modulation of adhesion, including activation of latent-TGFβs in the ECM. Quantitative sequencing of the brain endothelial cell transcriptome identifies TGFβ-regulated genes with putative links to blood vessel morphogenesis, including several genes linked to Wnt/β-catenin signaling. These results reveal that the β8 integrin cytoplasmic domain is essential for the regulation of TGFβ-dependent gene expression in endothelial cells and suggest that cross-talk between TGFβs and Wnt pathways is crucial for neurovascular development.

KEY WORDS: Latent-TGFβ, Endothelial cell, Angiogenesis, Neuroepithelial, Wnt, Perivascular astrocyte, Mouse

INTRODUCTION

Members of the αv family of integrins, comprising αvβ1, αvβ3, αvβ5, αvβ6 and αvβ8, bind with high specificity to RGD peptide motifs present in select extracellular matrix (ECM) proteins (McCarty, 2020). Embryos null for the αv integrin gene (*Itgav*) or β8 integrin gene (*Itgb8*), and thus lacking the αvβ8 integrin heterodimer, develop nearly identical phenotypes that include aberrant brain angiogenesis and intracerebral hemorrhage (Bader et al., 1998; McCarty et al., 2002; Zhu et al., 2002) that initiate in the ganglionic eminences of the midbrain. Conditional deletion of *Itgav* or *Itgb8* using Nestin-Cre (Tronche et al., 1999) leads to similar angiogenic pathologies as those that develop in *Itgav*−/− and *Itgb8*−/− embryos (Arnold et al., 2012, 2019, 2014; Hirota et al., 2015, 2011; Lee et al., 2015; Mobley and McCarty, 2011; Mobley et al., 2009). The major ligands for αvβ8 integrin in the brain are latent-TGFβs, which are embedded in the ECM as inactive latent complexes (Worthington et al., 2011). Integrin-induced conformational changes in the latent-TGFβ complex leads to cytokine release, engagement with TGFβ receptors and activation of canonical signaling events involving Smad transcription factors (Dong et al., 2014; Shi et al., 2011). Genetically targeting TGFβ receptor genes in endothelial cells, and particularly *Tgfbr2*, which encodes the type 2 TGFβ receptor, leads to CNS vascular pathologies that are strikingly similar to those that develop in mice lacking Itgav or Itgb8 in neuroepithelial cells (Allinson et al., 2012; Nguyen et al., 2011).

Integrin engagement with the ECM is regulated largely by inside-out activation, which involves a conformational transition from a low affinity inactive state to a high affinity ECM binding state. Inside-out activation is controlled by interactions between the β subunit cytoplasmic tail, intracellular signaling effectors and the cytoskeleton (Kadry and Calderwood, 2020). Structural studies of αvβ8 integrin, however, reveal that it exists mainly in an atypical adhesion-competent conformation termed 'extended-closed', rather than in a mixture of 'bent' (inactive) or 'extended' (active) conformations detected in other integrins (Wang et al., 2017). The extended-closed αvβ8 integrin structure suggests that a transition to a fully extended conformation might depend on regulatory components that interact with the transmembrane and/or cytoplasmic domain. Interestingly, the cytoplasmic tail of β8 integrin is divergent from other integrins (McCarty et al., 2005a) and lacks conserved sequences that recruit signaling effectors that function in inside-out activation (Chen et al., 2006; Jannuzi et al., 2004; Mathew et al., 2012; Menezes et al., 2014).

The unique properties of the β8 integrin cytoplasmic domain raise many questions about its roles in regulating intracellular signaling as well as ECM adhesion. For example, the cytoplasmic domain could serve to promote a transition from the extended-closed conformation to a fully active conformation with higher affinity ECM binding. Alternatively, the β8 integrin extracellular domain may be fixed in the extended-closed conformation, with the cytoplasmic tail having no roles in inside-out activation. Indeed, cell-based assays (Mu et al., 2002) and cryogenic electron microscopy studies of αvβ8 integrin (Campbell et al., 2020; Cormier et al., 2018) reveal that engagement with latent-TGFβ and activation of TGFβ signaling occurs independently of the cytoplasmic tail. Thus far, all *Itgb8* gene targeting approaches have generated complete loss-of-function mutants that do not distinguish roles for the cytoplasmic domain from the extracellular ECM binding domain in regulating neurovascular development and physiology.

Here, Cre/lox strategies in mice have been used to selectively delete the Itgb8 cytoplasmic domain while keeping the transmembrane and extracellular domains functionally intact. Mutant mice develop brain vascular pathologies that are linked to impaired latent-TGFβ activation and signaling in vascular

Department of Neurosurgery and Brain Tumor Center, Unit 1004, University of Texas MD Anderson Cancer Center, 1515 Holcombe Boulevard, Houston, Texas 77030, USA.

*Author for correspondence (jhmccarty@mdanderson.org)

J.H.M., 0000-0002-8345-5478

DEVELOPMENT

endothelial cells. We also detect unique cell signaling defects in the cytoplasmic domain-deficient mice that are distinct from complete loss-of-function (*Itgb8*−/−) mutants. Whole-transcriptome sequencing reveals that integrin activation of TGFβ signaling in brain vascular endothelial cells leads to changes in angiogenic gene expression, including alterations in several genes with links to canonical Wnt signaling. Collectively, these data establish a key function for the β8 integrin cytoplasmic tail in both extracellular adhesion and intracellular signaling in brain neurovascular units. These results also suggest that inhibition of the cytoplasmic domain may be an effective therapy for blocking ECM adhesion and activation of the TGFβ pathway.

RESULTS

Analysis of the murine β8 integrin protein sequence revealed that amino acids 682-702 constitute the transmembrane domain, with the final 65 amino acids (702-767) comprising the cytoplasmic domain. Amino acids 673-727 are encoded by *Itgb8* exon 13 and amino acids 728-767 are encoded by exon 14. Thus, by following

a standard Cre/lox knockout approach, the deletion of exons 13 and 14 would ablate both the β8 integrin transmembrane domain and the cytoplasmic domain. We assumed that perturbing the transmembrane domain would likely be problematic, as in other integrins this domain is involved in cell surface expression and heterodimerization with the αv subunit (Yang et al., 2009). Alternatively, inserting loxP sites flanking exon 14 alone would not result in the removal of the entire cytoplasmic domain. Therefore, we chose a strategy involving insertion of a premature STOP codon in exon 13 of the *Itgb8* gene to prevent expression of the downstream cytoplasmic sequences (Fig. 1A). To avoid potential dominant negative effects of the knock-in, we also inserted a cDNA mini-gene comprising exon 13/14 coding sequences and a polyA tail flanked by loxP sites upstream of exon 13 containing the engineered STOP codon. Cre-mediated deletion of the mini-gene enables transcriptional readthrough to the premature STOP in exon 13, leading to a truncated β8 integrin (ConKO/β8Δcyto). Correct *Itgb8* targeting was confirmed by Southern blotting and PCR-based analysis of purified genomic DNA (Fig. 1B,C). Deletion of the
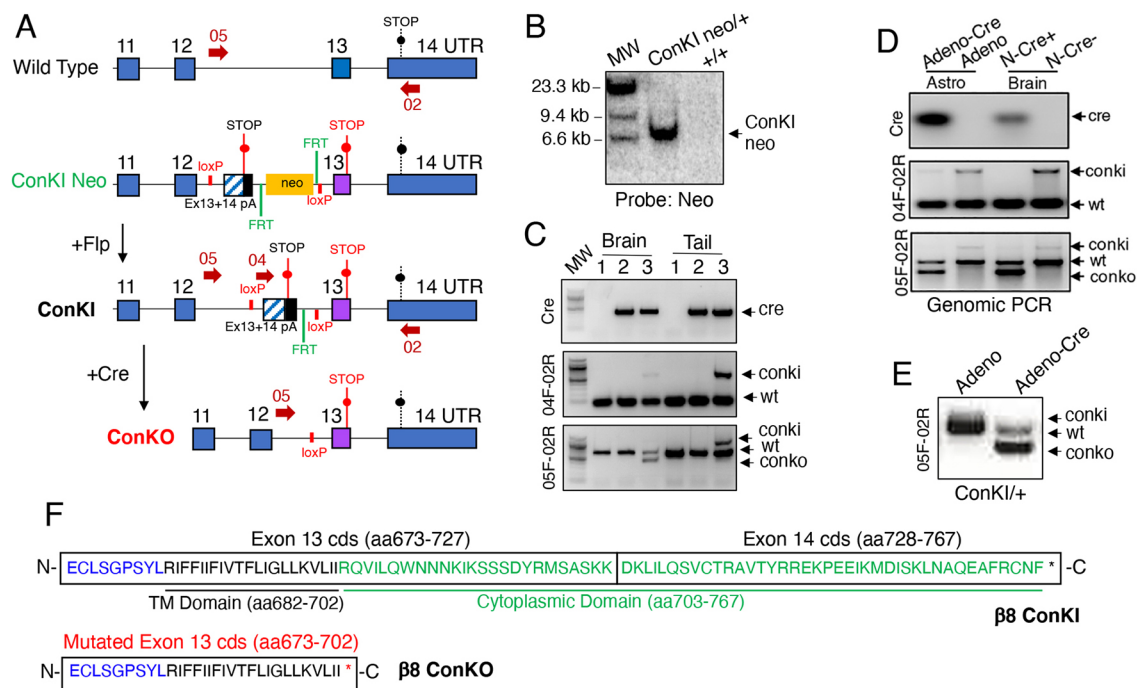

Fig. 1. Development of a Cre/lox mouse model to selectively delete the Itgb8 cytoplasmic domain. (A) General strategy for targeting the murine *Itgb8* gene to inhibit expression of the cytoplasmic domain. The 3′ region of the wild type *Itgb8* gene is shown at top with the endogenous STOP codon in exon 14. A premature STOP codon was knocked into exon 13. A floxed 'mini-gene' comprising a cDNA containing exon 13 and the coding sequence of exon 14 as well as a 3′ poly-A (pA) sequence was inserted upstream of the knock-in exon to avoid potential dominant-negative effects of the engineered STOP (ConKI-Neo). The Neo cassette was subsequently removed using Flp recombinase to generate the conditional knock-in allele (ConKI). Cre-mediated deletion of the floxed mini-gene sequence results in premature termination of translation (via the engineered STOP in exon 13) and generation of the conditional knockout allele (ConKO), which encodes a truncated protein that lacks the cytoplasmic domain. (B) Southern blot of genomic DNA isolated from wild-type control of ConKI Neo/+ heterozygote mice, digested with BamHI and hybridized with a probe corresponding to the Neo cassette. (C) Genomic PCR analysis using DNA isolated from E14 brain and tail tissue samples confirms correct targeting and Cre-mediated recombination at the *Itgb8* ConKI locus. Sample identities from brain and tail tissues in C are as follows: lane 1, Nestin-Cre−;+/+ (Cre-negative, wild type); lane 2, Nestin-Cre+;+/+ (Cre-positive, wild type); lane 3, Nestin-Cre+;ConKI/+ (Cre-positive, mutant). Forward and reverse DNA primer pairs used for PCR (05-02 and 04-02) are shown in the schematic (arrows in A). Note that Cre-mediated recombination occurs in the brain samples, but not in the tail samples. (D) Cortical astrocytes (Astro) cultured from mouse pups were infected with control adenovirus (Adeno) or Adeno-Cre and recombination at the engineered *Itgb8* ConKI allele was analyzed with PCR. Alternatively, dissected brain tissue from E18 ConKI/+ control (N-Cre−) or Nestin-Cre;ConKO/+ mice (N-Cre+) was analyzed by genomic PCR. Primer pairs used for genomic PCR analyses are shown by red arrows in A. (E) Cre-mediated recombination excises the mini-gene (Ex13/14), as confirmed by RT-PCR using RNA isolated from ConKI/+ brain neurospheres infected with control Adeno or Adeno-Cre. (F) Schematic showing the amino acid sequences for the β8 integrin transmembrane domain (black) and cytoplasmic domain (green) and corresponding exon 13 and 14 coding sequences (cds) of the wild-type *Itgb8* allele or the engineered *Itgb8* ConKI allele containing the mini-gene insertion (β8 ConKI, upper panel). The black asterisk indicates the endogenous STOP codon. Cre-mediated deletion of the loxP-flanked mini-gene allows transcriptional read through to a STOP codon engineered in exon 13, leading to termination of the Itgb8 coding sequence and truncation of the β8 integrin cytoplasmic domain (ConKO, lower panel). The red asterisk indicates the inserted premature STOP codon shown in panel A.

ConKI cassette was also confirmed using neurospheres cultured from control and ConKI/+ mice and infected with adenovirus-Cre (Fig. 1D). We also bred a Nestin-Cre transgenic strain (Tronche et al., 1999) to ConKI/+ mice to selectively delete the β8 integrin cytoplasmic domain in neuroepithelial cells of the developing brain. We confirmed that Nestin-Cre is active in neuroepithelial cells of the embryonic brain as early as E11, as revealed with the Rosa26-loxSTOPlox-YFP reporter (Fig. S1). As shown in Fig. 1D, genomic PCR analysis of neurospheres isolated from E14 control and Nestin-Cre;ConKO/+ embryonic brain validated Cre-mediated deletion of the mini-gene and resulting β8 integrin protein truncation. This result is similar to the deletion of the floxed mini-gene using cultured neurospheres infected with adenovirus-Cre (Fig. 1E). A schematic summary of the β8 integrin transmembrane and cytoplasmic sequences encoded by exons 13 and 14 as well as the expression of truncated β8 integrin protein resulting from Cre-mediated removal of the mini-gene is highlighted in Fig. 1F. Sanger sequencing was performed using cDNA prepared from Nestin-Cre control and Nestin-Cre;ConKO/+ E14 neurospheres, confirming Cre-mediated deletion of the floxed mini-gene and premature termination of the *Itgb8* cytoplasmic domain-coding sequence (Fig. S2).

Next, we generated a rabbit polyclonal antibody directed against the extracellular domain of β8 integrin. This antibody, as well as additional anti-αv and anti-β8 antibodies directed against cytoplasmic sequences, were used to test expression of αvβ8 integrin before and after Cre-mediated recombination (Fig. 2A). Immunoblot analysis of whole-brain lysates revealed a ∼93 kDa truncated protein expressed by the ConKO allele as well as a ∼100 kDa full-length protein expressed by the ConKI or wild-type allele (Fig. 2B). Truncated β8 integrin protein was not detected in samples that lacked the Nestin-Cre transgene. A second β8 integrin antibody developed against the cytoplasmic tail revealed expression of only the full-length β8 integrin protein (Fig. 2B). Immunoblotting for αv integrin protein did not reveal differences in expression after truncation of β8 integrin. We also analyzed αv and β8 integrin expression in neurospheres isolated from embryonic

day (E) 14 Nestin-Cre control and Nestin-Cre;ConKO/+ embryos. Immunoblot analysis revealed diminished levels of full-length β8 integrin protein in Nestin-Cre;ConKO/+ samples owing to mutation of one *Itgb8* allele (Fig. S3). We also cultured neurospheres from the brains of adult ConKI/+ mice and infected them with adenovirus control or adenovirus-Cre to induce β8 integrin protein truncation. Diminished levels of full-length β8 integrin protein were detected following adenovirus-Cre infection (Fig. S3). Neuroepithelial cells give rise to astrocyte progenitors in the postnatal brain (Toutounchian and McCarty, 2017; Verkhratsky and Nedergaard, 2018); therefore, we next examined whether cultured astrocyte progenitors from control and Nestin-Cre;ConKO/+ mice could bind to different ECM substrates using *in vitro* adhesion assays. As shown in Fig. 2C, in comparison with control cells, Nestin-Cre;ConKO/+ cells displayed defective adhesion to ECM proteins including collagen IV and fibronectin. Analysis of β8−/− cells revealed a similar deficiency in adhesion to ECM proteins (Fig. S3). Collectively, these data reveal that selective loss of the β8 integrin cytoplasmic domain leads to defects in cell-ECM adhesion.

Next, neurovascular development was analyzed *in vivo* using F1 progeny resulting from Nestin-Cre/+ males mated with ConKI/ConKI or ConKI/+ females. Nestin-Cre;ConKO/+ mutant mice were born in expected Mendelian ratios and did not display obvious developmental abnormalities (26 mutants of 115 total mice). Like controls, Nestin-Cre;ConKO/+ mutants did not develop obvious brain vascular pathologies such as intracerebral hemorrhage or hydrocephalus (Fig. 3A,B) that was grossly evident in β8−/− mutant embryos (Fig. 3C). The lack of severe brain vascular pathologies was not due to poor Nestin-Cre transgene expression or enzymatic activities, as conditional deletion of the β8flox/flox allele, and thus leading to CNS-specific Itgb8 loss-of-function, resulted in grossly obvious intracerebral hemorrhage (Fig. S4). Microscopic analyses of E14 brains, and particularly midbrain regions including the ganglionic eminences in Nestin-Cre;ConKO/+ mutants, revealed defective blood vessel patterning (Fig. 3D-F). Control brain sections showed close juxtaposition between neuroepithelial cells and radially migrating angiogenic
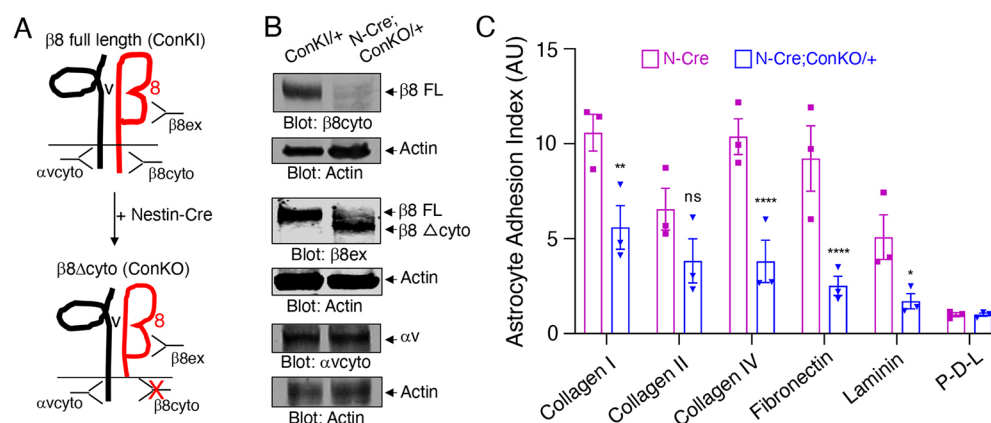

Fig. 2. The β8 integrin cytoplasmic domain promotes adhesion to the ECM. (A) Summary of antibodies directed against different regions (extracellular or cytoplasmic) of αv or β8 integrin proteins. Note that the β8cyto antibody cannot recognize the truncated β8 integrin protein (ConKO) owing to deletion of the cytoplasmic domain, whereas the β8ex antibody can recognize both the full-length (FL) and truncated β8 proteins. (B) Brain lysates from control (ConKI/+) or Nestin-Cre;ConKO/+ neonatal mice (P0) were analyzed by immunoblotting with antibodies directed against the β8 integrin extracellular domain (β8ex), the β8 integrin cytoplasmic domain (β8cyto) and the αv integrin cytoplasmic domain (αvcyto). (C) Quantification of β8 integrin cytoplasmic domain-dependent adhesion to various ECM proteins. Astrocyte progenitors from Nestin-Cre control or Nestin-Cre;ConKO/+ brains were added to wells coated with the indicated ECM proteins (x-axis) and cell adhesion was quantified after 16 h. Note that loss of the β8 integrin cytoplasmic tail leads to defects in ECM adhesion. Differences between groups were analyzed using two-way ANOVA and Tukey post-hoc analysis (n=3, mean±s.e.m., *P<0.05, **P<0.01, ****P<0.0001). ns, not significant.
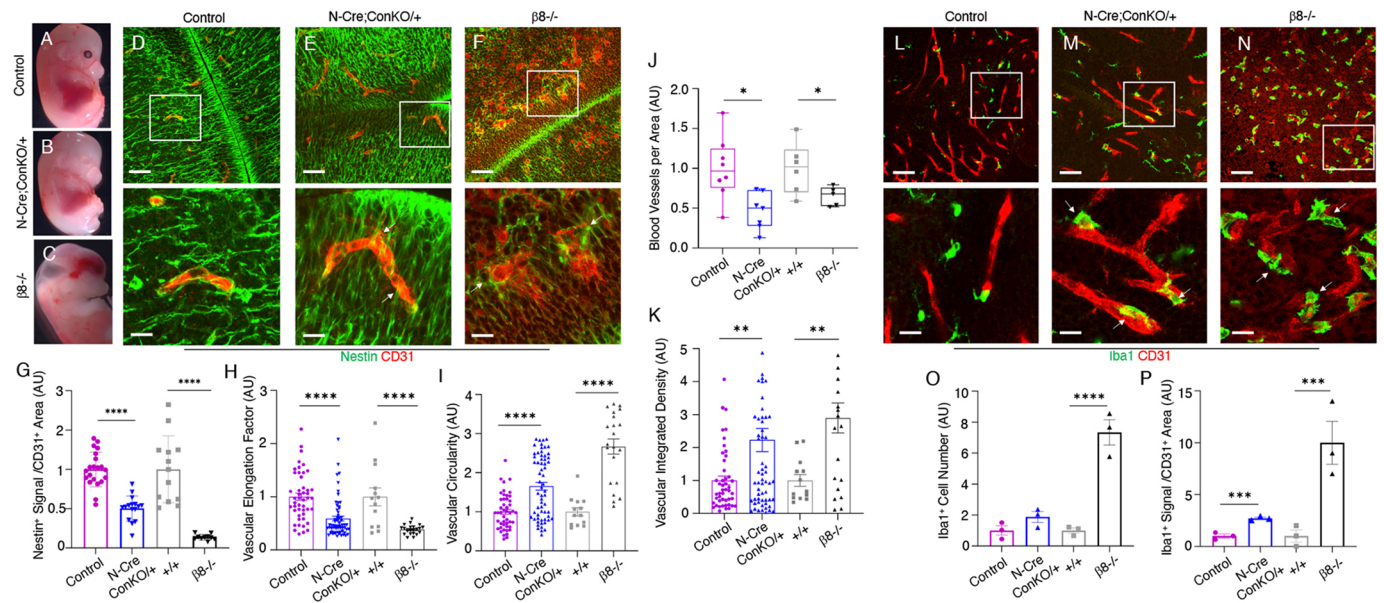
Fig. 3. Deletion of the β8 integrin cytoplasmic domain leads to defective cell adhesion and aberrant blood vessel morphogenesis during brain development. (A-C) Representative images of E14 Nestin-Cre control (A), Nestin-Cre;ConKO/+ (B) and β8−/− (C) embryos. Note that unlike β8−/− embryonic brains, which are hemorrhagic and hydrocephalic, there is a lack of grossly obvious hemorrhage in Nestin-Cre;ConKO/+ embryos. (D-F) Sagittal sections through the ganglionic eminence regions of E14 Nestin-Cre control (D), Nestin-Cre;ConKO/+ (E) or β8−/− embryos (F) were analyzed by double immunofluorescence using anti-CD31 antibody (red) to detect vascular endothelial cells combined with anti-nestin (green) antibody to detect neuroepithelial cells. Note that, in comparison to blood vessels in control mice, microscopic analysis of blood vessels in the Nestin-Cre;ConKO/+ and β8−/− brains reveal abnormal, distended morphologies as well as disrupted contacts with perivascular neuroepithelial cells. The lower panels are higher magnified images of boxed areas in upper panels. (G) Quantitation of neuroepithelial-endothelial cell juxtaposition in the ganglionic eminences of E14 Nestin-Cre control versus Nestin-Cre;ConKO/+ mutant embryos as well as wild-type control versus β8−/− mutant embryos. (H,I) Quantitation of blood vessel morphologies in the ganglionic eminences of E14 Nestin-Cre control versus Nestin-Cre;ConKO/+ mutant embryos and wild-type control versus β8−/− mutant embryos. Note the significant decrease in vascular elongation along the neuroepithelium (H) and a corresponding increase in circularity indicative of shape defects (I). The β8−/− mutant mice brains revealed similar alterations in cerebral blood vessel morphology. (J) Quantitation of blood vessels per area in the ganglionic eminences of control and mutant mice. Note the decrease in the number of CD31^{+} blood vessels per area in Nestin-Cre;ConKO/+ and β8−/− mutant embryos compared with the controls. (K) Quantitation of blood vessel shapes within the ganglionic eminences of control, Nestin-Cre;ConKO/+ and β8−/− mutant embryos. In comparison with controls, CD31^{+} blood vessels in mutant brains were more dilated. Aberrantly shaped blood vessels covered larger areas and thus showed enhanced anti-CD31 fluorescence intensity, as characterized by higher integrated density values. (L-N) Sagittal sections through midbrain regions of E14 Nestin-Cre control (L), Nestin-Cre;ConKO/+ (M) or β8−/− embryos (N) were analyzed by double immunofluorescence using anti-CD31 (red) antibody to detect vascular endothelial cells combined with anti-Iba1 (green) antibody to detect microglial cells. Note that in comparison to blood vessels in control mice, the blood vessels in the Nestin-Cre;ConKO/+ and β8−/− brains have abnormal morphologies and show increased juxtaposition with microglia. The lower panels are higher magnified images of boxed areas in upper panels. (O,P) Quantitation of perivascular microglial cells in the ganglionic eminences of E14 control and mutant embryos. In comparison to control mice, a higher number of Iba1^{+} cells was identified near blood vessels in Nestin-Cre;ConKO/+ mutant mice brains. The β8−/− mutant brain sections contained higher numbers of total microglia and perivascular microglia. Differences between groups were analyzed using unpaired two-tailed Student's *t*-test (*n*=3, mean±s.e.m., *P<0.05, **P<0.01, ***P<0.001, ****P<0.0001). Scale bars: 20 μm (D-F,L-N, upper panels); 5 μm (D-F,L-N, lower panels).

blood vessels (Fig. 3D,G). In contrast, cerebral blood vessels in Nestin-Cre;ConKO/+ mutants did not closely juxtapose the neuroepithelium, as revealed by double immunofluorescence imaging with anti-nestin and anti-CD31 antibodies (Fig. 3E,G). In addition, brain endothelial cells in the Nestin-Cre;ConKO/+ mutants did not sprout radially along neuroepithelial cell processes and displayed abnormal morphologies, as determined by several quantitative parameters (Fig. 3H-K). The *in vivo* adhesion and sprouting abnormalities support the *in vitro* defects in cell-ECM binding (Fig. 2C). Lastly, although total numbers of microglia were not significant in control versus Nestin-Cre;ConKO/+ mutant mice, there were increased numbers of perivascular microglial cells in mutants, as revealed by double labeling with anti-Iba1 and anti-CD31 antibodies (Fig. 3L-O). In particular, significantly higher numbers of Iba1^{+} microglial cells were detected near distended blood vessels in ganglionic eminences of the midbrain (Fig. 3P). Analysis of E18 embryos revealed lack of macroscopic intracerebral hemorrhage in Nestin-Cre;ConKO/+ mice compared with controls, whereas hemorrhage was obvious in β8−/− embryos (Fig. S4). However, in E18 Nestin-Cre;ConKO/+ mutants there

were continued defects in the juxtaposition between vascular endothelial cells and neuroepithelial cells (Fig. S5). Cerebral blood vessels in E18 Nestin-Cre;ConKO/+ mutant mice were associated with increased numbers of microglia, as revealed by labeling with anti-Iba1 antibodies (Fig. S5). Similar to controls, vascular endothelial cells in Nestin-Cre;ConKO/+ and β8−/− mutant brains were associated with pericytes, as revealed by double immunofluorescence with anti-CD31 and anti-NG2 antibodies (Fig. S5).

Integrin-dependent TGFβ activation and signaling via Smad transcription factors was next analyzed in control and mutant E14 brains. As shown in Fig. 4A-G, reduced levels of Smad3 phosphorylation were detected in blood vessels within Nestin-Cre; ConKO/+ mutant brains, as revealed by immunofluorescence staining of fixed sections with anti-CD31 and a phospho-specific Smad3 antibody. There was also significantly less phosphorylated Smad3 in brain endothelial cells of β8−/− embryonic brain sections (Fig. 4H-N). We also detected reduced levels of phospho-Smad3 in vascular endothelial cells in Nestin-Cre;β8flox/flox conditional knockout brains (Fig. S6). Collectively, these data reveal that the
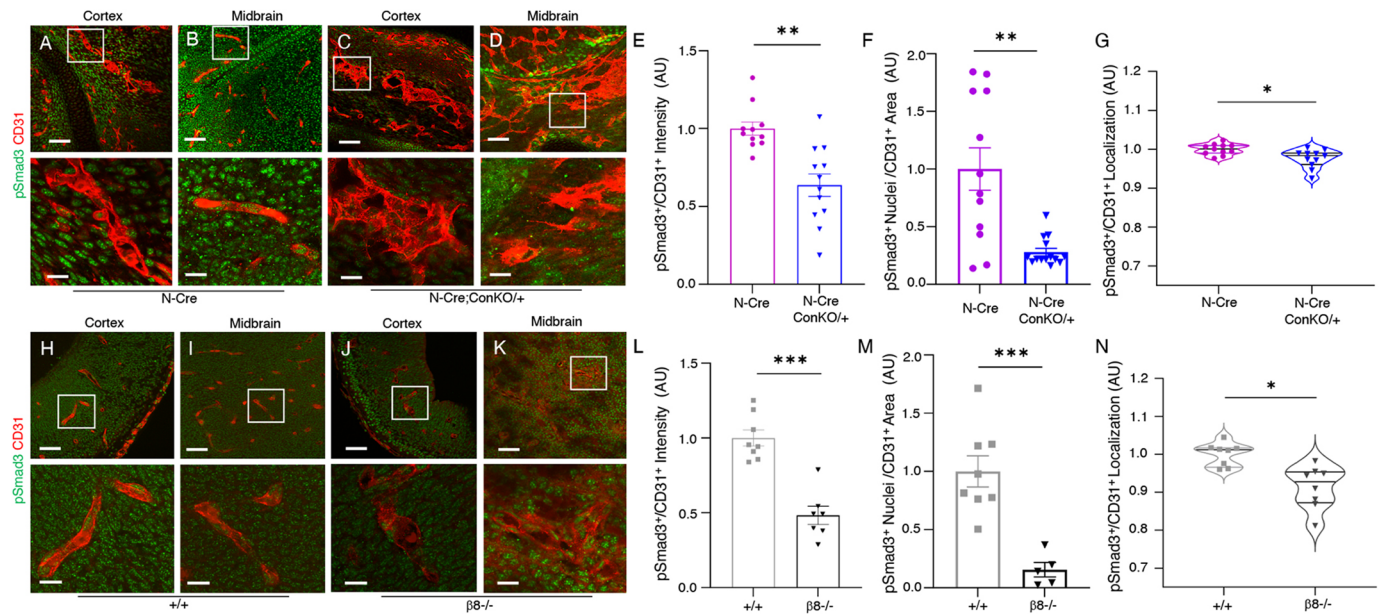
Fig. 4. Deletion of β8 integrin cytoplasmic domain in brain neuroepithelial cells leads to reduced TGFβ-Smad signaling in vascular endothelial cells.
(A-D) Analysis of Smad3 phosphorylation in brains from E14 Nestin-Cre control (A,B) and Nestin-Cre;ConKO/+ embryos (C,D). Shown are sagittal sections through the forebrains/cerebral cortices (A,C) and the ganglionic eminence regions of the midbrain (B,D). Note the abnormal CD31$^+$ blood vessel morphologies in Nestin-Cre;ConKO/+ brains with reduced levels of pSmad3. The lower panels are higher magnification images of boxed areas in upper panels. (E-G) Quantification of pSmad3 levels in E14 Nestin-Cre control and Nestin-Cre;ConKO/+ midbrain regions as plotted in a bar graph measuring fluorescence intensity of pSmad3 relative to CD31 (E), numbers of pSmad3$^+$ nuclei normalized to total CD31$^+$ area (F) or by violin plots showing pSmad3$^+$/CD31$^+$ co-localization (G). Note the reduced levels of pSmad3 in Nestin-Cre;ConKO/+ brain samples. (H-K) Analysis of Smad3 phosphorylation in brains from E14 wild-type control (+/+; H,I) and β8−/− embryos (J,K). Shown are sagittal sections through the developing cerebral cortices (H,J) and the ganglionic eminence regions of the midbrain (I,K). Note the abnormal CD31$^+$ blood vessel morphologies in β8−/− brains with defects in levels of pSmad3. The lower panels are higher magnification images of boxed areas in upper panels. (L-N) Quantification of pSmad3 levels in E14 wild-type control and β8−/− midbrain regions as plotted in a bar graph measuring fluorescence intensity of pSmad3 relative to CD31 (L), numbers of pSmad3$^+$ nuclei normalized to total CD31$^+$ area (M) or by violin plots showing pSmad3$^+$/CD31$^+$ co-localization (N). Differences between groups were determined using unpaired two-tailed Student's t-test (n=3, mean±s.e.m., $*P<0.05$, $**P<0.01$, $***P<0.001$). Violin plots show distribution of statistically comparable mean values by analyzing differences between control and mutant brains (n=3 per group). Scale bars: 20 μm (A-D,H-K, upper panels); 5 μm (A-D,H-K, lower panels).

vascular pathologies in the Nestin-Cre;ConKO/+ mutant brains are most likely related to defects in TGFβ signaling in vascular endothelium.

Using *in vitro* cell-based assays, β8 integrin-dependent activation of latent-TGFβs was also quantified. Purified LAP-TGFβ1 was added to wild-type or mutant astrocyte progenitors and conditioned media was subsequently transferred to HEK-293T reporter cells expressing a Smad binding element-inducible secreted alkaline phosphatase reporter construct (SBE-iSEAP) (Fig. 5A). As shown in Fig. 5B, conditioned medium from Nestin-Cre control cells that had been pre-treated with exogenous LAP-TGFβ1 induced robust SBE-iSEAP activities in a time-dependent manner. Conversely, conditioned medium from Nestin-Cre;ConKO/+ astrocyte progenitors treated with exogenous LAP-TGFβ1 induced lower levels of SBE-iSEAP activities (Fig. 5B). Similarly, reduced latent-TGFβ1 activation and signaling was detected in β8−/− cells using the SBE-iSEAP reporter assay (Fig. 5C).

To identify signaling pathways that are linked to the β8 integrin cytoplasmic tail we used the antibody-based reverse-phase protein array (RPPA) platform (Nishizuka and Mills, 2016). Astrocyte progenitor cultures were prepared from postnatal day (P) 0 wild-type mice (adhesion, transmembrane and signaling domains intact), β8−/− mice (adhesion, transmembrane and signaling domains deleted) and Nestin-Cre;ConKO mice (signaling domain deleted) and detergent-soluble lysates were tested using RPPA (Fig. 6A). These cultures mostly comprised Nestin$^+$/GFAP$^+$ astrocyte progenitors, but also contained some vascular endothelial cells and

microglia (Tchaicha et al., 2010). Several signaling proteins involved in growth, polarity and/or migration were differentially expressed or phosphorylated in cultured astrocyte progenitors lacking the β8 integrin cytoplasmic domain (Fig. 6B). Interestingly, the levels of these proteins were inversely correlative in β8−/− samples versus Nestin-Cre;ConKO/+ samples (Fig. 6C). For example, in comparison with controls, the ECM protein collagen VI showed elevated expression in Nestin-Cre;ConKO/+ lysates and reduced expression in β8−/− lysates. These data suggest that complete loss of adhesion and signaling domains (β8−/−) versus selective loss of only the signaling domain (Nestin-Cre;ConKO/+) have differential impacts on protein expression and/or stability. Next, we tested expression of collagen VI and the GTP exchange factor Vav1 identified by RPPA by immunoblotting detergent-soluble lysates from control and mutant cells. As shown in Fig. 6D, in Nestin-Cre;ConKO/+ astrocyte progenitor lysates we detected elevated expression of collagen VI as well as reduced expression of Vav1. Quantitation of these immunoblot data show integrin-dependent changes in expression that are consistent with the RPPA results (Fig. 6E). Lastly, in comparison with Nestin-Cre control littermates, immunohistochemical staining of P0 brain sections revealed increased expression of collagen VI protein throughout the cerebral cortex of Nestin-Cre;ConKO/+ mutants (Fig. S7).

Although Nestin-Cre;ConKO/+ mutant mice displayed microscopic angiogenesis defects during embryonic and neonatal development, all mutant animals analyzed thus far (n=11) have survived to adulthood (>1 year) without the onset of age-related
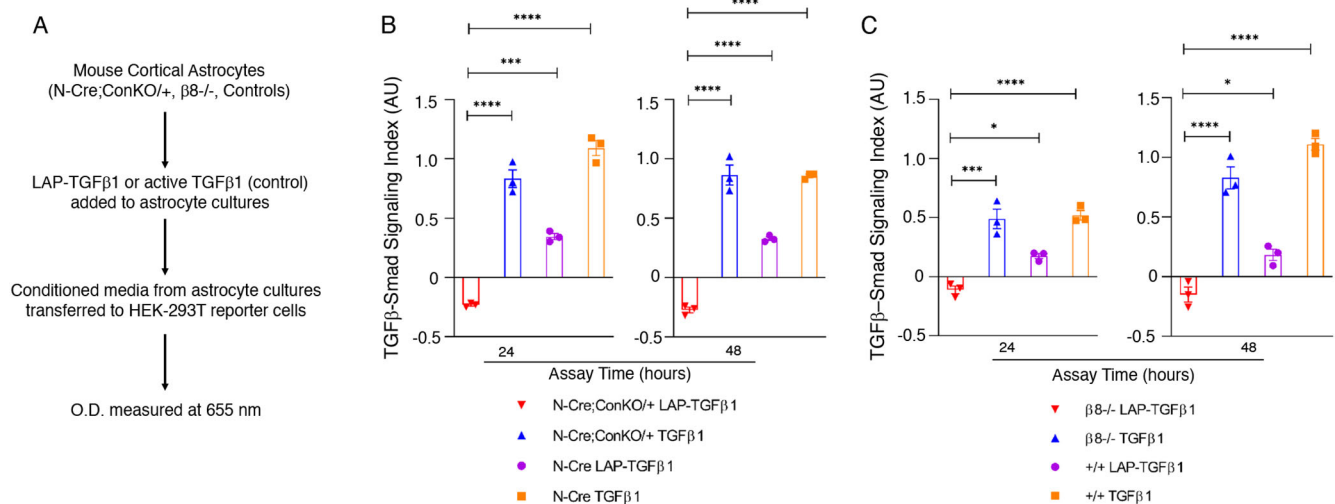
Fig. 5. The β8 integrin cytoplasmic domain promotes latent-TGFβ activation *in vitro*. (A) Experimental strategy for quantifying β8 integrin-dependent latent-TGFβ activation and signaling *in vitro* using control and mutant astrocytes and HEK-293 cells expressing SBE-iSEAP reporter constructs. (B,C) Quantification of β8 integrin-mediated activation of latent-TGFβ1 using Nestin-Cre control and Nestin-Cre;ConKO/+ astrocytes (B) as well as wild-type and β8−/− astrocytes (C) in cell-based SBE-iSEAP reporter assays. Astrocyte conditioned media (+/− exogenous LAP-TGFβ1 or bioactive TGFβ1) was transferred to HEK-SBE Blue cells followed by quantification of reporter activities at 24 and 48 h. Note that both Nestin-Cre;ConKO/+ and β8−/− astrocytes show reduced latent-TGFβ activation and signaling at 24 and 48 h in comparison with control astrocytes. Differences between groups were analyzed using unpaired two-tailed Student's *t*-test (*n*=3, mean±s.e.m., **P*<0.05, ****P*<0.001, *****P*<0.0001).

neurological defects. Nestin-Cre;ConKO/+ adult mice showed reduced body weights in comparison with age-matched controls (Fig. 7A); however, there were no neurodegenerative phenotypes or obvious motor deficits as assessed with a Rotarod (Fig. 7B). The normal postnatal survival as well as the lack of obvious neurological deficits in Nestin-Cre;ConKO/+ mice are unlike the diminished survival of β8−/− or Nestin-Cre;β8flox/flox mice, which die by 6 months owing to spinocerebellar neurodegeneration (McCarty et al., 2005b; Mobley and McCarty, 2011; Mobley et al., 2009). Microscopic analysis of brain sections from adult Nestin-Cre; ConKO/+ mutant mice did not reveal persistent defects in blood vessel morphologies, and differences in astrocytes and microglia were not apparent (Fig. 7C-H). In contrast, adult β8−/− and Nestin-Cre;β8flox/flox mutant brains (P60) showed increased numbers of astrocytes and microglial cells (Fig. S8). Interestingly, analysis of brains from neonatal (P10) Nestin-Cre;ConKO/+ mutants did not reveal microscopic hemorrhage, although we detected increased numbers of astrocytes in the cortex and striatum, as revealed by immunohistochemistry for GFAP (Fig. S9). A previous report has shown that intracerebral hemorrhage in β8−/− and Nestin-Cre; β8flox/flox mice leads to microglial activation and subsequent motor dysfunction (Arnold et al., 2019). However, we did not detect obvious differences in Iba1^{+} microglial cell numbers in Nestin-Cre; ConKO/+ at P10, although β8−/− mice of a similar age displayed microhemorrhage and increased numbers of perivascular glial cells (Fig. S9).

Collectively, our results reveal that, during development, the β8 integrin cytoplasmic domain promotes activation of ECM-bound latent-TGFβs and subsequent TGFβ receptor signaling in endothelial cells (Figs 2-5). These data are consistent with previous reports showing that deletion of the *Tgfbr2* gene, which encodes the type 2 TGFβ receptor, in vascular endothelial cells using a tamoxifen-inducible endothelial cell-specific Cre transgenic model, Cdh5-CreERT2, leads to similar angiogenesis pathologies (Allinson et al., 2012). We also detected abnormal angiogenesis and microscopic hemorrhage when the *Tgfbr2* gene is acutely

ablated in vascular endothelial cells using the PDGFB-CreERT2 model (Fig. 8A-F). The *Tgfbr2*-regulated genes and pathways in the brain vascular endothelium that control developmental angiogenesis remain largely unknown; therefore, we performed quantitative RNA-sequencing (RNA-seq) to identify differentially expressed genes in *Tgfbr2*−/− brain endothelial cells. To facilitate sorting of endothelial cells we also intercrossed *Tgfbr2* flox/flox mice with Cre-inducible ROSA26-loxSTOPlox-EYFP (R26-EYFP) reporter mice (Mao et al., 2001). Neonatal mice were injected with tamoxifen once per day for three consecutive days, and vascular endothelial cells were isolated from freshly dissected P7 brains based on YFP and CD31 expression (Fig. 8G). As shown in Fig. 8H,I and Fig. S10, several genes showed differential expression in *Tgfbr2*+/− control versus *Tgfbr2*−/− cells. Five genes (*Mfsd2a*, *ApoD*, *Htra3*, *Spock2* and *Wfdc1*) identified to be downregulated in *Tgfbr2*−/− brain endothelial cells were independently validated by qRT-PCR (Fig. 8J). Analysis of the brainrnaseq.org database confirmed enriched expression of these five genes in brain vascular endothelial cells isolated from P7 mice (Fig. S11). Stimulation of the bEnd.3 brain endothelial cell line with TGFβ1 led to significantly increased expression of four of the five genes analyzed (Fig. 8K). We have previously shown TGFβ1-dependent regulation of *Mfsd2a* expression in brain endothelial cells (Tiwary et al., 2018). Interestingly, other reports have shown that expression of *ApoD*, *Htra3*, *Spock2* and *Wfdc1* (Jensen et al., 2019) as well as *Mfsd2a* (Wang et al., 2020) is controlled by canonical Wnt signaling. Therefore, we treated brain endothelial cells with Wnt7a and analyzed expression of these five genes. As shown in Fig. 8L, we confirmed Wnt-dependent increase in expression of four of the five genes, with levels of *Htra3* not impacted by Wnt7a treatment.

Collectively, these data reveal that the β8 integrin cytoplasmic domain is necessary for neuroepithelial cell adhesion to ECM protein ligands, and particularly latent-TGFβs, in the brain microenvironment. Our results support a model in which engagement of the β8 integrin cytoplasmic sequences with the cytoskeleton and/or intracellular effector proteins is essential for the

DEVELOPMENT
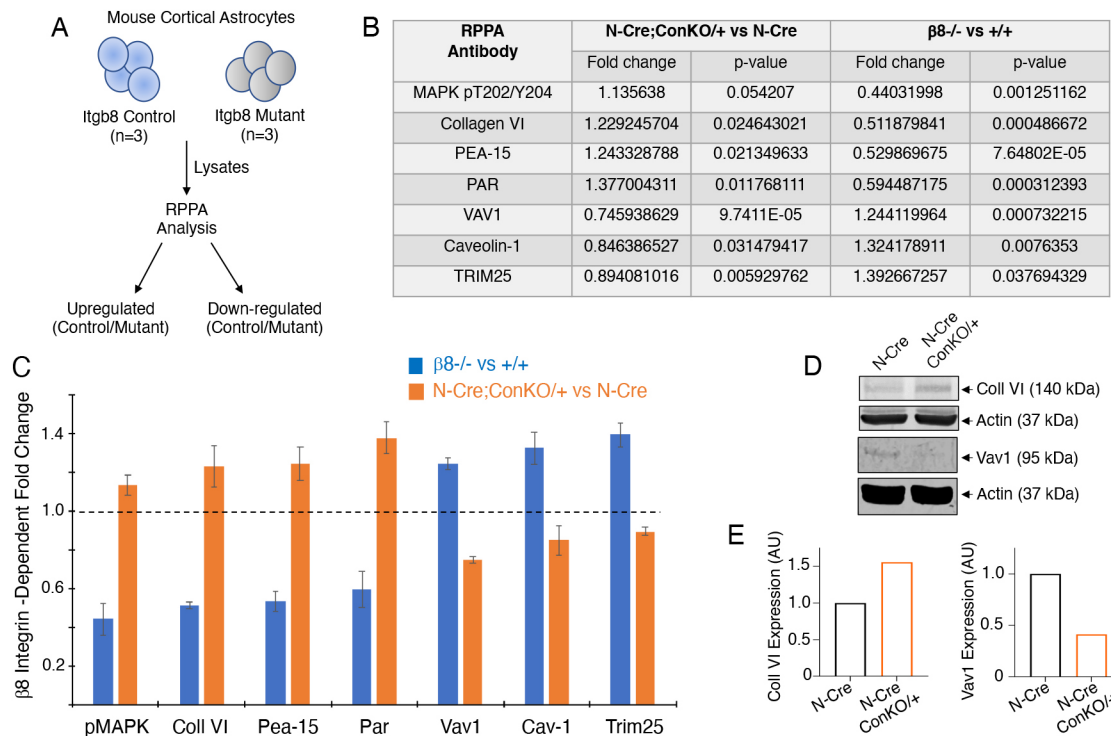
Fig. 6. The β8 integrin cytoplasmic domain regulates signal transduction in cultured glial cells. (A) Strategy to identify β8 integrin-dependent changes in protein expression or phosphorylation in mouse astrocytes using reverse phase protein array (RPPA) platforms. (B) Table summarizing the seven most differentially expressed and/or phosphorylated proteins (with relevant *P*-values) in mutant versus control astrocytes identified by RPPA. (C) Bar graph summarizing select proteins that show statistically significant differences in expression and/or phosphorylation in control versus β8−/− astrocytes or Nestin-Cre control versus Nestin-Cre;ConKO/+ astrocytes. Shown are the top seven proteins displaying differential expression and/or phosphorylation in mutant cells. Note the inverse correlation between expression and/or phosphorylation of the seven proteins in astrocyte progenitors cultured from Nestin-Cre;ConKO/+ versus β8−/− pups. Data are mean±s.d. (D) Detergent-soluble lysates from Nestin-Cre control and Nestin-Cre;ConKO/+ mutant astrocytes were immunoblotted using anti-collagen VI and anti-Vav1 antibodies. Note the integrin-dependent changes in expression, which correlates with the expression differences identified in the RPPA screen (B,C). (E) Densitometry-based quantification of collagen VI (left) and Vav1 (right) protein levels based on immunoblot data in D.
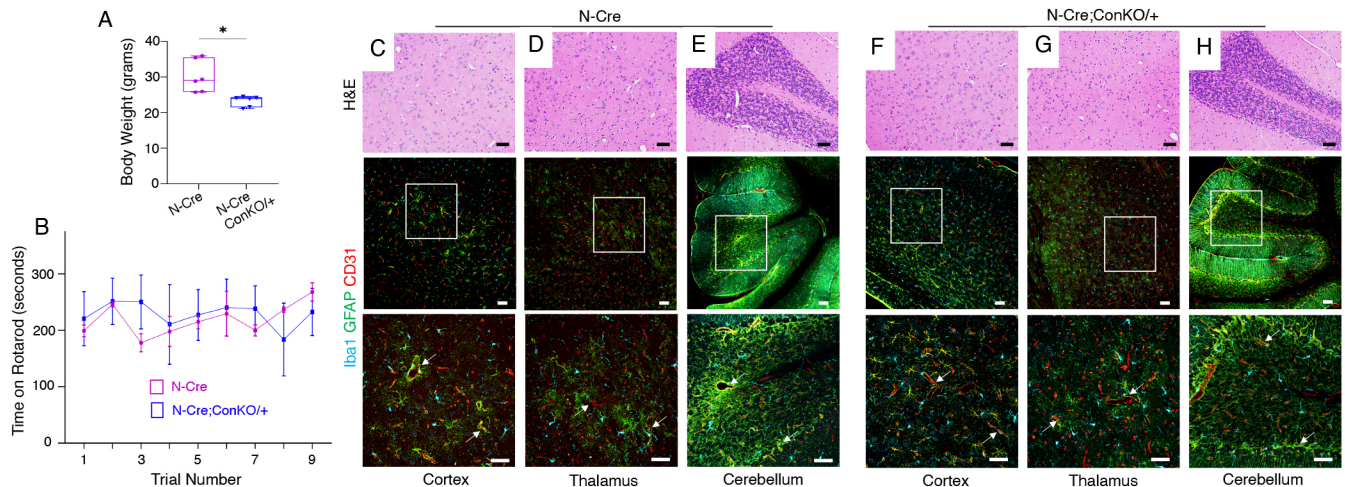

Fig. 7. Absence of brain vascular pathologies and neurodegenerative phenotypes in adult Nestin-Cre;ConKO/+ mice. (A) Body weights were recorded for 7 month old male Nestin-Cre control and Nestin-Cre;ConKO/+ mice. Unpaired two-tailed Student's *t*-test was used to compare differences between groups (*n*=3, mean±s.e.m., *P<0.05). Box and whisker plot shows distribution of statistically comparable minimum and maximum values (boxes) around mean (middle bars) as determined by quantifying differences between control and mutant groups (*n*=3 mice per group). (B) Rotarod analyses of 7 month old male Nestin-Cre control (*n*=3) and Nestin-Cre;ConKO/+ mutant mice (*n*=3). The time (*y*-axis) the mice remained on the rod rotating at an increasing speed versus the trial number (*x*-axis) is plotted. Note the lack of statistically significant differences in time spent on the rod for mutant versus control mice. (C-H) Sagittal brain sections from 7 month old Nestin-Cre control (C-E) or Nestin-Cre;ConKO/+ mutant mice (F-H) through the cerebral cortex (C,F), thalamus (D,G) and cerebellum (E,H) were stained with Hematoxylin and Eosin (upper panels) or fluorescently labeled with anti-Iba1 (cyan), anti-GFAP (green) and anti-CD31 (red) antibodies (lower panels) to reveal microglia, astrocytes and vascular endothelial cells, respectively. Note the absence of obvious neurovascular pathologies in Nestin-Cre;ConKO/+ mutant brain sections (F-H). White arrows in the fluorescent panels indicate blood vessels with closely juxtaposed astrocytes and/or microglial cells. The lower panels are higher magnification images of the boxed areas within the middle panels. Scale bars: 50 μm.

DEVELOPMENT

Fig. 8. β8 integrin-activated TGFβ signaling regulates gene expression in brain endothelial cells. (A-F) Images of brains and fixed sections from tamoxifen-injected Pdgfbb-CreERT2 control (A) or Pdgfbb-CreERT2;*Tgfbr2*f/f conditional knockout (B) mice stained with Hematoxylin and Eosin (C,D) or anti-CD31 and anti-GFAP antibodies (E,F). Note that Pdgfbb-CreERT2;*Tgfbr2*f/f mutant mice develop focal brain hemorrhages and angiogenesis defects (arrows in B,D) as well as higher numbers of perivascular astrocytes (arrows in F). Mice received three consecutive intragastric tamoxifen injections between P1 and P3 and were analyzed at P7. (G) Strategy to identify TGFβ-regulated genes involved in cerebral angiogenesis and neurovascular development. Bulk transcriptome sequencing was performed on YFP^{+}/CD31^{+} brain endothelial cells (ECs) isolated from P7 PDGFBB-CreERT2f/+;R26-YFP/+ control or PDGFBB-CreERT2;*Tgfbr2*f/f;R26-YFP/+ inducible knockout (iCKO) mice. (H) Heat map listing the top differentially expressed genes in control Pdgfbb-CreERT2;*Tgfbr2*f/+;R26-YFP/+ (*n*=3) and mutant Pdgfbb-CreERT2;*Tgfbr2*f/f;R26-YFP/+ (*n*=5) brain endothelial cells. (I) Decreased relative expression of five select genes (*Mfsd2a*, *Apod*, *Htra3*, *Spock2*, *Wfdc1*) as measured by quantitative mRNA sequencing from isolated control and *Tgfbr2*−/− brain endothelial cells. (J) Quantitative RT-PCR analysis validates differential expression in control and *Tgfbr2*−/− brain endothelial cell samples for five genes identified from transcriptome sequencing. (K) Brain endothelial cells (bEnd.3) were treated with TGFβ1 for 12 h and expression of *Tgfbr2*, *Mfsd2a*, *ApoD*, *Htra3*, *Spock2* and *Wfdc1* was quantified by RT-PCR. (L) Brain endothelial cells were treated with Wnt7a for 24 h and expression levels of *Tgfbr2*, *Mfsd2a*, *ApoD*, *Htra3*, *Spock2* and *Wfdc1* mRNAs were quantified by RT-PCR. Statistical differences of means were determined by two-way ANOVA (*n*=3, mean±s.e.m.). **P*<0.05, ***P*<0.01, ****P*<0.001, *****P*<0.0001.

propagation of the extended-closed conformation and possibly the generation of novel ECM adhesion-competent conformations in αvβ8 integrin (Fig. 9). These results also indicate that functionally blocking the β8 integrin cytoplasmic domain may be an effective strategy for perturbing ECM adhesion, including inhibition of the TGFβ pathway.

DISCUSSION

Most integrin β subunits, including β1A, β2, β3A, β5 and β6, use NPXY motifs in their cytoplasmic domains to recruit talins and/or kindlins, which induce dramatic inside-out structural changes in the extracellular region that convert the inactive conformation to ECM binding-competent conformations (Ginsberg, 2014). In contrast, the

Fig. 9. Model for the β8 integrin cytoplasmic tail in control of ECM adhesion and intracellular signaling. Activated full-length αvβ8 integrin promotes ECM engagement and clustering, leading to enhanced avidity to protein ligands and robust intracellular signaling. Genetic deletion of the β8 cytoplasmic domain impairs intracellular signaling and cytoskeletal linkages. αvβ8Δcyto is shown in a clustered complex with full-length αvβ8 integrin (ConKO/+). This figure was created with BioRender.com.

β8 integrin cytoplasmic tail lacks NPXY motifs and its isolated extracellular region is detected mainly in an extended-closed conformation that can bind effectively to ECM ligands (Dong et al., 2014; Wang et al., 2017). It will be important to further elucidate the cytoplasmic domain-dependent mechanisms that propagate the extended-closed state or convert it to a more active conformation, including the relative contributions of intracellular proteins that interact with the β8 integrin cytoplasmic tail. For example, the F-actin binding protein band 4.1B (McCarty et al., 2005a) could control cytoskeleton-dependent alterations in αvβ8 integrin ECM adhesion. Alternatively, PTP-PEST could dynamically promote extracellular adhesion via reversible control of integrin phosphorylation (Lee et al., 2015) or RhoGDI1-mediated Rac1/Cdc42 activation (Reyes et al., 2013). The β8 integrin cytoplasmic tail might also mediate interactions with endothelial cell-expressed neuropilin 1 (Nrp1), which is linked to TGFβ receptor signaling and is a counter-receptor for αvβ8 integrin (Hirota et al., 2015). Altered interactions between αvβ8 integrin and Nrp1 might result in impaired neuroepithelial-endothelial cell adhesion leading to aberrant activation of latent TGFβ and/or TGFβ receptor signaling in endothelial cells. Nrp1 is also expressed at lower levels in the developing brain neuroepithelium, and the cytoplasmic domain of Nrp1 binds to PDZ domain-containing proteins (Lanahan et al., 2013). Interestingly, spinophilin, which binds to the β8 integrin cytoplasmic tail (Cheerathodi et al., 2016), contains a PDZ domain that may mediate associations between Nrp1 and αvβ8 integrin.

The RPPA experiments using lysates from astrocyte progenitor cultures reveal differential expression of collagen VI, Vav1 and other factors, indicating that αvβ8 integrin controls the expression and/or stability of these proteins. In the adult mouse brain, however, *Vav1* and *Col6a1* mRNAs are enriched in microglia and fibroblasts, respectively (Vanlandewijck et al., 2018). It is possible that these cells are admixed in the astrocyte cultures, with αvβ8 integrin promoting intercellular adhesion and communication between astrocytes and other stromal cells. Indeed, perivascular microglia play important roles in regulating brain angiogenesis (Paredes et al., 2018). Alterations in αvβ8 integrin functions might affect the morphology and activation status of nearby microglia, possibly involving leucine rich repeat containing protein 33 (LRRC33). LRRC33, an extracellular protein secreted into the microenvironment by microglia, is essential for latent-TGFβ activation, possibly through cooperative binding with αvβ8 integrin in perivascular astrocytes (Qin et al., 2018).

The quantitative RNA-seq results and cell signaling data reveal novel cross-talk mechanisms between TGFβs and Wnts in vascular endothelial cells. Previous reports have shown that β-catenin plays a crucial role in vascular development, particularly in the brain (Liebner et al., 2008). Selective ablation of *Wnt7a*/*Wnt7b* genes in neuroepithelial cells, or *Ctnnb1*/β-catenin in endothelial cells (Daneman et al., 2009; Stenman et al., 2008), leads to brain angiogenesis pathologies that are similar to those that develop in *Itgav*, *Itgb8* or *Tgfbr2* mutant mice (McCarty, 2009). Norrin, which has structural homology to TGFβs but signals via Wnt receptors, regulates developmental angiogenesis in the brain and retina (Wang et al., 2018). Inhibition of Wnt/β-catenin signaling in brain endothelial cells during development revealed significant downregulation of several ECM genes with links to the TGFβ pathway (Jensen et al., 2019). A more recent report has shown cross-talk between TGFβs and Wnts in vascular endothelial cells during retinal angiogenesis and formation of the blood-retina barrier (Zarkada et al., 2021). The proteins GPR124 and Reck are also

linked to Wnt signaling and it will be important to determine whether this complex is linked to αvβ8 integrin adhesion and signaling pathways (Vallon et al., 2018). In cancer, cross-talk between TGFβ/Smad signaling and Wnt/β-catenin signaling occurs at multiple levels to regulate gene expression (Attisano and Labbe, 2004). The Smad3 C-terminal region interacts with β-catenin to form a Smad4/Smad3/β-catenin complex following engagement of TGFβ1 with the TGFβ receptor complex (Tian and Phillips, 2002; Zhang et al., 2010). Our data identify specific genes that are regulated via cross-talk between TGFβs and Wnts in the brain endothelium. It will be interesting to further dissect these interactions in development and also determine whether these events are altered in vascular-related neurological disorders.

MATERIALS AND METHODS
Experimental mice
All animal protocols were reviewed and approved before use by the Institutional Animal Care and Use Committee (IACUC) and The University of Texas MD Anderson Cancer Center Subcommittee on Animal Studies, both AAALAC accredited institutions. Details for generating Nestin-Cre; β8$^{flox/flox}$ conditional knockout and β8$^{-/-}$ whole body knockout have been reported previously (Mobley et al., 2009; Proctor et al., 2005). A conditional knock-in model was generated by insertion of a premature STOP codon within one of the exons coding for cytoplasmic domain of β8 integrin and a floxed cDNA (mini-gene) upstream. For Southern blot experiments, genomic DNA isolated from wild-type control of ConKI Neo/+ heterozygote mice was digested with BamHI, resolved by electrophoresis and blots were hybridized with a probe corresponding to the Neo cassette. Such conditional knock-in females (ConKi/+) were bred with Nestin-Cre/+ males to achieve Cre/lox removal of two coding exon sequences along with an intervening intron coding for β8 integrin cytoplasmic tail, thus generating conditional knockout mice (Nestin-Cre/+;β8-ConKi/+) that harbored a truncated form of β8 integrin in neuroepithelial cells. The Nestin-Cre transgenic mice (Tronche et al., 1999) were purchased from Jackson Laboratories (stock 003771). ROSA26-loxSTOPlox-EYFP mice were also purchased from Jackson Laboratories (stock 006148). The PDGFB-CreERT2 (Claxton et al., 2008) and *Tgfbr2*flox/flox (Nguyen et al., 2011) models have been described previously. Mouse genotypes were confirmed by genomic DNA isolation from ear snips and standard PCR protocols. Embryo staging involved timed mating, with the morning of the plug date defined as E0. For mouse behavioral analyses, a Rotarod device (Ugo Basile) was used to measure motor coordination and strength. The times at which mice fell from the rod were recorded. Mice were allowed to stay on the rod for a maximum of 360 s (6 min). Six separate trials were performed over a 3-day period (three trials per day).

Tissue sectioning, immunofluorescence and immunohistochemistry
Embryonic and neonatal mouse brains were harvested and fixed in cold 4% paraformaldehyde (15714, Electron Microscopy Sciences) in 1× PBS (21-040-CV, Corning and SH30256.01, Hyclone) for 15 h at 4°C. Fixed brains were washed with 1× PBS and embedded in 4.5% low melting point agarose (16520, Invitrogen, Life Technologies) for embryonic brains or 3% agarose (GR140, Denville Scientific) for postnatal brains. Embedded brains were sectioned under ice-cold conditions using a vibratome (VT 1000S, Leica) to collect 100 μm sagittal or coronal brain slices. Tissue sections were blocked using 0.25% Triton X-100 (Fisher BioReagents) in 1× PBS containing 10% species-specific serum (Jackson ImmunoResearch Laboratories) matching the secondary antibody host. Commercially available primary and secondary antibodies (Table S1) were used for immunostaining. Brain tissue sections were mounted using Vectashield antifade mounting medium (H-1200, Vector Laboratories). For all immunohistochemistry, heat-induced antigen retrieval was performed using 1× sodium citrate buffer (pH 6.0) (C9999, Millipore Sigma) or 1 mM EDTA (pH 8.0) (unless otherwise indicated as per manufacturer's instructions). Permeabilization of brain tissue sections (formalin-fixed paraffin embedded), was performed using

0.1% Triton X-100 in 1× PBS, followed by blocking with 10% species-specific serum (Jackson ImmunoResearch Laboratories) matching the secondary antibody host (Jackson ImmunoResearch Laboratories) for both immunohistochemistry and immunofluorescence, and developed using ImmPACT DAB substrate, peroxidase (HRP, SK-4150, Vector Laboratories) for immunohistochemistry. Primary and secondary antibodies used are included in Table S1. Bright-field microscopy was performed using Carl Zeiss Axio Imager.Z1 and Olympus BX43 microscopes.

Image acquisition, analysis and quantitation
Immunofluorescence images were acquired using Olympus FLUOVIEW FV3000 confocal laser scanning microscope. Multi-dimensional acquisition was carried out using z-stacks with 2.5 μm slicing intervals at a scan rate of 4 μs/pixel with a resolution of at least 1024×1024 pixels per slice and digitally compiled in FV31S-SW (ver. 2.4.1.198). Image acquisition parameters including laser power, exposure time, voltages and gain were assigned uniformly across experimental and control samples for each imaging channel. All images were analyzed using Fiji and Image J software packages (Schindelin et al., 2012; Schneider et al., 2012) and serial z-stack images (three 2.5 μm slices per image) were used for all quantification. Multiple areas of different brain regions were imaged across experimental and control mice groups (n=3). Fluorescence intensity of pSmad3$^+$ nuclei and CD31$^+$ blood vessel signals were measured from corresponding channels using the standard 'analyze color histogram' module. Blood vessel adjacent regions were analyzed for quantitating nestin$^+$ neuroepithelial cell contacts with CD31$^+$ blood vessels, and pSmad3$^+$/CD31$^+$ co-localization. Digitally magnified microscopic images were used to manually draw around blood vessels using the 'freehand tool' and fluorescence signal co-localization was quantitated using the 'co-localization' algorithm in Fiji. Mander's correlation coefficients of signal co-localization were measured with or without background-corrected threshold values. A similar approach was adopted to quantify pSmad3$^+$ nuclei by using digitally magnified microscopic images and manually drawing around CD31$^+$ vascular areas. Similar threshold parameters were used for all images from both control and mutant brains and pSmad3$^+$ nuclei were counted using the 'analyze particles' algorithm in Fiji (Kumari and Rana, 2015). Numbers of pSmad3$^+$ nuclei were normalized to the total CD31$^+$ vascular area.

All images were scaled (μm) as per the objective lens used for acquisition to measure cellular parameters. Acquired image stacks were projected for maximum intensity to include all signals, but the auto-threshold module was then used to include only cellular signals for quantitation and exclude non-specific background or noise. CD31$^+$ blood vessel parameters (counts, area coverage, mean fluorescence signal intensity) were quantified using the 'vessel analysis' module in Fiji (Simms et al., 2017). Numbers of perivascular microglial cells were quantitated by measuring Iba1$^+$ cell parameters in both low magnified microscopic images to include larger brain regions and digitally magnified images to include areas adjacent to CD31$^+$ blood vessels. Cell counts, area coverage, mean fluorescence signal intensity, major and minor axes for shape descriptors, and cell circularity were analyzed using the 'analyze particles' algorithm (Kumari and Rana, 2015). Iba1$^+$ cells were counted above the set threshold of 50 μm^2 to avoid any non-specific background or noise. Integrated density parameter measures total cellular fluorescence intensity per cell area. A cell with higher area coverage and/or mean signal intensity gives increased integrated density values. Maximum and minimum distances between two points on the cell periphery are defined by the major and minor axes (McWhorter et al., 2013). A completely circular cell will have identical major and minor axes values, whereas the difference between the major and minor axes will change in accordance with cell shape alterations. For example, the difference between the major and minor axes will be larger when a cell becomes less circular and attains more ameboid or elongated morphology. Shape factor determines such differences between major and minor cellular axes to validate dynamic transitions in cell morphology.

Mouse astrocyte progenitors and brain endothelial cell line cultures
Neonatal brains (P1-P3) were harvested and cerebral cortices were carefully collected after removal of meninges and other structures including the hippocampus. Cortical sheets were minced and washed in sterile 1 g/l (low glucose) Dulbecco's Modified Eagle's Medium (DMEM) with L-glutamine and sodium pyruvate (10-014-CV, Corning) by centrifugation at 1000 rpm (150 **g**) for 5 min at room temperature (RT). Tissue pellets were re-suspended and gently agitated in fresh and sterile DMEM containing 150 U/ml of collagenase (Type I, LS004196, Worthington Biochemical) and 40 μg/ml of DNAse I (D7291, Sigma-Aldrich) for 30 min at 37°C. After centrifugation at 1000 rpm for 5 min at RT, the pellet was re-suspended in sterile astrocytic growth medium [1 g/l DMEM containing 10% bovine calf serum (BCS; SH30072.03, Hyclone) and 1 U/ml Penicillin-Streptomycin (MT30004CI, Corning)], and triturated. The suspension was filtered through a 40 μm nylon cell strainer (Falcon) and 10 ml of suspension was added to T-75 tissue culture flasks (Corning), pre-coated with laminin from Engelbreth-Holm-Swarm murine sarcoma basement membrane (L2020, Sigma-Aldrich), used at 1:300 dilution in sterile 1× PBS. Primary astrocyte progenitor cultures were maintained (37°C, 5% CO$_2$) by replacing with fresh and sterile astrocytic growth medium every 3-4 days until they were confluent. Mouse brain endothelial cells (bEnd.3; ATCC) were maintained in DMEM (30-2002, ATCC) containing 10% fetal bovine serum (F0926, Sigma-Aldrich) and 1% antibiotic-antimycotic solution (30-004-CI, Corning). Cells were serum starved overnight at confluence and treated with either 1 ng/ml recombinant human TGFβ1 protein (7754-BH, R&D Systems) for 12 h or 50 ng/ml human Wnt7a protein (GTX53868-pro, GeneTex) for 24 h.

TGFβ-Smad reporter assays
HEK293T cell line, stably transfected with human *TGFBR1*, *SMAD3* and *SMAD4* genes, was purchased from InvivoGen (hkb-tgfb). This HEK-Blue™ TGFβ SEAP reporter cell line detects bioactive TGFβ through activation of downstream TGFβ-Smad signaling pathway and production of detectable secreted alkaline phosphatase protein (SEAP). Cells were grown and passaged (according to manufacturer's instructions) in sterile 4.5 g/l (high glucose) DMEM (10-017-CV, Corning) containing 10% heat-inactivated fetal bovine serum (F4135, Sigma-Aldrich), 1 U/ml Penicillin-Streptomycin and 100 μg/ml Normocin™ (InvivoGen), and maintained through selection (according to manufacturer's instructions) by the same growth medium but containing 30 μg/ml Blasticidin™ (ant-bl, InvivoGen), 200 μg/ml Hygromycin B gold™ (ant-hg, InvivoGen) and 100 μg/ml Zeocin™ (ant-zn, InvivoGen). Cells were passaged (trypsin-free) every 3-4 days or when they were ~75% confluent. Primary astrocyte progenitors cultured from neonatal mice brains were used to measure their ability to activate latent TGFβ1, thus generating bioactive TGFβ. Confluent astrocytic cultures were passaged by 0.25% trypsin, 0.1% EDTA in HBSS (without calcium, magnesium and sodium bicarbonate; MT 25053CI, Corning), and cells collected by centrifugation (1000 rpm, 5 min at RT) were re-suspended in fresh sterile astrocyte growth medium (heat-inactivated 10% BCS used for assay) and counted (Vi-cell Analyzer, Beckman Coulter). Then 1×10^5 viable astrocytes were seeded per well of a 12-well tissue culture plate (Corning), pre-coated with laminin from Engelbreth-Holm-Swarm murine sarcoma basement membrane (L2020, Sigma-Aldrich) used at 1:300 dilution in sterile 1× PBS, and containing 1 ml of growth medium per well. Cells were allowed to grow (37°C, 5% CO$_2$) for 3-4 days. Growth medium was replaced with 1 g/l DMEM containing 10% BCS (heat-inactivated), 1 U/ml Penicillin-Streptomycin, and conditioned with 1 ng/ml latent-TGFβ1 (rh-Latent-TGFβ1, 299-LT/CF, R&D Systems), 1 ng/ml active TGFβ (7754-BH-005/CF, R&D Systems), and no TGFβ (control). All TGFβ treatments were carried out in triplicates and cells were conditioned for 15 h at 37°C and 5% CO$_2$. Concurrently, antibiotics-selected Hek-Blue TGFβ cells were passaged at 75% confluence in T-75 tissue culture flasks using the methods described above. Passaged cells were grown for 15 h (37°C, 5% CO$_2$) on a 48-well tissue culture plate (Corning) with 2×10^5 viable cells/ml/well. After 15 h of incubation, growth medium was replaced by conditioned medium from astrocytic cultures (described above) and HEK-blue-TGFβ cells were further incubated at 37°C, 5% CO$_2$. Then 20 μl of cell supernatant was collected from each well independently at 24, 48 and 72 h and added to one well of a 96-well plate. After adding 180 μl of Quanti-blue™ assay reagent (rep-qbs, InvivoGen) per well containing cell supernatant, the cells were incubated at 37°C for 15-60 min. Finally,

10

absorbance (O.D.) was measured at 655 nm (Synergy HTX multi-mode reader, BioTek).

Adenovirus infection of cells

Control or ConKI/+ neurospheres were grown in serum-free media and infected either with Ad5 adenovirus expressing Cre (UIOWA, Ad5CMVCre) or control adenovirus (UIOWA, Ad5CMVempty). After initial titering of virus, a multiplicity of infection (MOI) of 100 was used to infect cells for 48 h for genomic PCR analysis or 4-7 days for immunoblot analysis.

ECM adhesion assays

Primary cell cultures from β8$^{−/−}$, Nestin-Cre/+;β8-ConKi/+ and paired wild-type (control) P0/P1 mice brains were passaged once they were confluent in T75 tissue culture flasks [pre-coated with laminin from Engelbreth-Holm-Swarm murine sarcoma basement membrane (L2020, Sigma-Aldrich) used at 1:300 dilution in sterile 1× PBS] containing astrocyte growth media. Standard cell culture technique involving 0.25% trypsin, 0.1% EDTA in HBSS (without calcium, magnesium and sodium bicarbonate; MT 25053CI, Corning) was used to detach cells followed by trypsin neutralization (#0113, ScienCell Research Laboratories), centrifugation (1000 rpm, 5 min, RT) and re-suspension of cell pellets in 2 mM EDTA (Invitrogen 15575020, Fisher Scientific) containing 1× PBS (RT). Re-suspended cells were washed again by centrifugation (1000 rpm, 5 min, RT) and re-suspended in 4 ml of assay buffer (ECM540, Millipore Sigma). Viable cell count was obtained (Vi-cell Analyzer, Beckman Coulter) and 2×10^4 viable cells were added per well of the 96-well strip (ECM540, Millipore Sigma). The assay was carried out using the ECM cell adhesion array kit (ECM540, Millipore Sigma) following the manufacturer's instructions. Final absorbance readings were taken at 650 nm (Synergy HTX multi-mode reader, BioTek).

Immunoblotting and immunoprecipitation

Confluent astrocyte progenitor cultures were lysed using radioimmunoprecipitation assay buffer [RIPA: 50 mM Tris-HCl (pH 8.0), 150 mM NaCl, 1% sodium deoxycholate, 1% Triton X-100, 0.1% SDS, 1% NP-40 and 1 mM EDTA] containing protease and phosphatase inhibitors (A32955, A32957, Thermo Fisher Scientific) to obtain soluble protein fractions. Total protein concentration in lysates was determined using bicinchoninic acid assay (Pierce™ BCA, 2327, Thermo Fisher Scientific). For western blot analysis, SDS-PAGE was performed with 7.5%, 10% or 12% polyacrylamide gels, under reducing or non-reducing conditions, transferred to nitrocellulose membranes (Bio-Rad) and blocked using Intercept® TBS blocking buffer (927-60001, LI-COR) or 3% milk in 1× PBS containing 0.2% Tween-20. For immunoprecipitation, cell surface proteins of confluent astrocyte cultures were biotinylated (EZ-link™ Sulfo-NHS-Biotin, 21217, Thermo Fisher Scientific) followed by quenching with 1× TBS (Tris-buffered saline, T60075-4000, RPI). Cells were lysed using the same protocol described above to obtain total soluble protein lysates and protein concentration was determined using BCA method. Then 100-200 μg of protein lysate was incubated overnight with 2.5-5 μg of primary antibody (Table S1) at 4°C, and 50-100 μl of Protein A agarose (11134515001, Roche) (washed with cold 1× PBS by centrifugation and finally re-suspended in RIPA buffer), was added per tube containing protein-primary antibody conjugates and incubated at 4°C for 1 h. The primary antibody-agarose conjugate was immunoprecipitated by centrifugation [15,000 rpm (21,400 g), 10 min, 4°C] and washed with RIPA buffer containing protease and phosphatase inhibitors. Finally, the pellet was re-suspended in non-reducing sample buffer and western blot analysis was performed using the same protocol described above. All primary and secondary antibodies used are included in Table S1. Immunoblots were scanned using Odyssey CLx infrared imaging system with Image Studio (LI-COR).

Reverse-phase protein arrays

Adherent cells were washed twice with ice-cold PBS, lysed in RIPA or RPPA lysis buffer containing 1% Triton X-100, 50 mM Hepes (pH 7.4), 150 mM NaCl, 1.5 mM MgCl$_2$, 1 mM EGTA, 100 mM NaF, 10 mM sodium pyruvate, 1 mM Na$_3$VO$_4$, 10% glycerol and a cocktail of protease and phosphatase inhibitors (Roche Diagnostics) for 20-30 min with frequent mixing on ice, centrifuged at 14,000 rpm (18,600 g) at 4°C for 15 min to isolate the detergent-soluble protein supernatant. The protein concentration was determined using the BCA assay (or Bradford) and the optimal protein concentration of lysates for RPPA was 1.2 mg/ml. Lysates were denatured in 4× sample buffer [35% glycerol, 8% SDS, 0.25 M Tris-HCl (pH 6.8); without β-mercaptoethanol] for 5 min at 95°C. Lysates were stored at −80°C and subsequently analyzed at RPPA core facility at the MD Anderson Cancer Center. Samples were serially diluted and probed with 466 antibodies and arrayed on nitrocellulose-coated slides. Relative protein levels were normalized for loading and compared with the standard curve. Normalized data points were transformed to a linear value used for analysis.

Isolation of primary mouse brain endothelial cells for transcriptomic profiling

PDGFBB-CreERT2f/+;*Tgfbr2*f/+;R26-YFP/+ control or PDGFBB-CreERT2;*Tgfbr2*f/f;R26-YFP/+ mutant were intragastrically injected with 50 mg tamoxifen (50 ml, 1 mg/ml) from P1 to P3. At P7, mice were euthanized by CO$_2$ in accordance with IACUC regulations. Mouse brains were dissected out under sterile conditions and all subsequent work was carried out within a tissue culture hood. The brains were manually dissociated and CD31$^+$ selected by use of fluorescence-activated cell sorting of CD31-APC and YFP$^+$ cells. Control (n=3) and mutant (n=5) cell samples were subsequently transcriptionally profiled using RNA-seq analysis. After RNA quality was validated, eight samples of a RNA integrity number (RIN) of ≥7 were loaded onto HiSeq400 instrument. An average of ~40 million paired-end reads were generated for each of the eight samples. Sequenced reads fastq files were mapped to mouse reference genome GRCm3 (mm10) using Tophat v2.0.13 (Kim et al., 2013). Raw reads count were calculated using HTseq 0.12.4 (Anders et al., 2015). Differentially expressed genes between control and *Tgfbr2* mutant cells were obtained using the edgeR package (Robinson et al., 2010). Differentially expressed genes are those having logFC>2 and FDR<0.01.

Cultured brain endothelial cell RNA extraction and quantitative real time PCR

Total RNA was extracted from both treated and untreated bEnd.3 cells using the RNeasy mini kit (74106, Qiagen) and quantified using NanoDrop 2000c (Thermo Fisher Scientific) spectrophotometer. cDNA was synthesized using ready-to-go you-prime first-strand beads (27926401, Cytiva) and random hexamers (N8080127, Invitrogen). Quantitative real time PCR was performed using iTaq™ Universal SYBR® Green Supermix (1725121, Bio-Rad) on a 7500 Fast Real-Time PCR system (Applied Biosystems). The qRT-PCR primers are listed in Table S2. The relative gene expression was quantified using the ΔΔCt method and fold changes of targeted genes were normalized by *Gapdh* mRNA. Expression level of targeted genes in the untreated bEnd.3 cells and/or wild-type mouse brain endothelial cells was taken as 1 and the other values are expressed as fold change over basal expression. Each sample was tested in triplicate. The RNA-seq files have been deposited online and are freely accessible at https://data.mendeley.com/datasets/3g8x5cmx6z/2.

Statistical analyses

Quantitation of confocal images were performed using ImageJ (National Institutes of Health) (Rueden et al., 2017; Schindelin et al., 2012). GraphPad prism 8.0 was used to plot mean values (n≥3±s.e.m., unless otherwise indicated) to compare between experimental and control groups and to determine statistical differences by unpaired two-tailed Student's *t*-test and two-way ANOVA (Tukey post-hoc analysis) at 95% confidence intervals (α value 0.05); *$P<0.05$, **$P<0.01$, ***$P<0.001$ and ****$P<0.0001$.

Competing interests

The authors declare no competing or financial interests.

DEVELOPMENT

References
Allinson, K. R., Lee, H. S., Fruttiger, M., McCarty, J. H. and Arthur, H. M. (2012). Endothelial expression of TGFβ type II receptor is required to maintain vascular integrity during postnatal development of the central nervous system. *PLoS ONE* **7**, e39336. doi:10.1371/journal.pone.0039336

Anders, S., Pyl, P. T. and Huber, W. (2015). HTSeq–a Python framework to work with high-throughput sequencing data. *Bioinformatics* **31**, 166-169. doi:10.1093/bioinformatics/btu638

Arnold, T. D., Ferrero, G. M., Qiu, H., Phan, I. T., Akhurst, R. J., Huang, E. J. and Reichardt, L. F. (2012). Defective retinal vascular endothelial cell development as a consequence of impaired integrin αVβ8-mediated activation of transforming growth factor-β. *J. Neurosci.* **32**, 1197-1206. doi:10.1523/JNEUROSCI.5648-11.2012

Arnold, T. D., Niaudet, C., Pang, M.-F., Siegenthaler, J., Gaengel, K., Jung, B., Ferrero, G. M., Mukouyama, Y.-S., Fuxe, J., Akhurst, R. et al. (2014). Excessive vascular sprouting underlies cerebral hemorrhage in mice lacking αVβ8-TGFβ signaling in the brain. *Development* **141**, 4489-4499. doi:10.1242/dev.107193

Arnold, T. D., Lizama, C. O., Cautivo, K. M., Santander, N., Lin, L., Qiu, H., Huang, E. J., Liu, C., Mukouyama, Y.-S., Reichardt, L. F. et al. (2019). Impaired alphaVbeta8 and TGFbeta signaling lead to microglial dysmaturation and neuromotor dysfunction. *J. Exp. Med.* **216**, 900-915. doi:10.1084/jem.20181290

Attisano, L. and Labbe, E. (2004). TGFbeta and Wnt pathway cross-talk. *Cancer Metastasis Rev.* **23**, 53-61. doi:10.1023/A:1025811012690

Bader, B. L., Rayburn, H., Crowley, D. and Hynes, R. O. (1998). Extensive vasculogenesis, angiogenesis, and organogenesis precede lethality in mice lacking all αv integrins. *Cell* **95**, 507-519. doi:10.1016/S0092-8674(00)81618-9

Campbell, M. G., Cormier, A., Ito, S., Seed, R. I., Bondesson, A. J., Lou, J., Marks, J. D., Baron, J. L., Cheng, Y. and Nishimura, S. L. (2020). Cryo-EM reveals integrin-mediated TGF-β activation without release from latent TGF-β. *Cell* **180**, 490-501.e16. doi:10.1016/j.cell.2019.12.030

Cheerathodi, M., Avci, N. G., Guerrero, P. A., Tang, L. K., Popp, J., Morales, J. E., Chen, Z., Carnero, A., Lang, F. F., Ballif, B. A. et al. (2016). The cytoskeletal adapter protein spinophilin regulates invadopodia dynamics and tumor cell invasion in glioblastoma. *Mol. Cancer Res.* **14**, 1277-1287. doi:10.1158/1541-7786.MCR-16-0251

Chen, H., Zou, Z., Sarratt, K. L., Zhou, D., Zhang, M. Z., Sebzda, E., Hammer, D. A. and Kahn, M. L. (2006). In vivo β1 integrin function requires phosphorylation-independent regulation by cytoplasmic tyrosines. *Genes Dev.* **20**, 927-932. doi:10.1101/gad.1408306

Claxton, S., Kostourou, V., Jadeja, S., Chambon, P., Hodivala-Dilke, K. and Fruttiger, M. (2008). Efficient, inducible Cre-recombinase activation in vascular endothelium. *Genesis* **46**, 74-80. doi:10.1002/dvg.20367

Cormier, A., Campbell, M. G., Ito, S., Wu, S., Lou, J., Marks, J., Baron, J. L., Nishimura, S. L. and Cheng, Y. (2018). Cryo-EM structure of the alphavbeta8 integrin reveals a mechanism for stabilizing integrin extension. *Nat. Struct. Mol. Biol.* **25**, 698-704. doi:10.1038/s41594-018-0093-x

Daneman, R., Agalliu, D., Zhou, L., Kuhnert, F., Kuo, C. J. and Barres, B. A. (2009). Wnt/beta-catenin signaling is required for CNS, but not non-CNS, angiogenesis. *Proc. Natl. Acad. Sci. USA* **106**, 641-646. doi:10.1073/pnas.0805165106

Dong, X., Hudson, N. E., Lu, C. and Springer, T. A. (2014). Structural determinants of integrin beta-subunit specificity for latent TGF-beta. *Nat. Struct. Mol. Biol.* **21**, 1091-1096. doi:10.1038/nsmb.2905

Ginsberg, M. H. (2014). Integrin activation. *BMB Rep.* **47**, 655-659. doi:10.5483/BMBRep.2014.47.12.241

Hirota, S., Liu, Q., Lee, H. S., Hossain, M. G., Lacy-Hulbert, A. and McCarty, J. H. (2011). The astrocyte-expressed integrin alphavbeta8 governs blood vessel sprouting in the developing retina. *Development* **138**, 5157-5166. doi:10.1242/dev.069153

Hirota, S., Clements, T. P., Tang, L. K., Morales, J. E., Lee, H. S., Oh, S. P., Rivera, G. M., Wagner, D. S. and McCarty, J. H. (2015). Neuropilin 1 balances

beta8 integrin-activated TGFbeta signaling to control sprouting angiogenesis in the brain. *Development* **142**, 4363-4373. doi:10.1242/dev.113746

Jannuzi, A. L., Bunch, T. A., West, R. F. and Brower, D. L. (2004). Identification of integrin β subunit mutations that alter heterodimer function in situ. *Mol. Biol. Cell* **15**, 3829-3840. doi:10.1091/mbc.e04-02-0085

Jensen, L. D., Hot, B., Ramsköld, D., Germano, R. F. V., Yokota, C., Giatrellis, S., Lauschke, V. M., Hubmacher, D., Li, M. X., Hupe, M. et al. (2019). Disruption of the extracellular matrix progressively impairs central nervous system vascular maturation downstream of beta-catenin signaling. *Arterioscler. Thromb. Vasc. Biol.* **39**, 1432-1447. doi:10.1161/ATVBAHA.119.312388

Kadry, Y. A. and Calderwood, D. A. (2020). Chapter 22: Structural and signaling functions of integrins. *Biochim. Biophys. Acta Biomembr.* **1862**, 183206. doi:10.1016/j.bbamem.2020.183206

Kim, D., Pertea, G., Trapnell, C., Pimentel, H., Kelley, R. and Salzberg, S. L. (2013). TopHat2: accurate alignment of transcriptomes in the presence of insertions, deletions and gene fusions. *Genome Biol.* **14**, R36. doi:10.1186/gb-2013-14-4-r36

Kumari, R. and Rana, N. (2015). Particle size and shape analysis using imagej with customized tools for segmentation of particles. *Int. J. Eng. Res. Technol.* **4**, 23-28. doi:10.17577/IJERTV4IS110211

Lanahan, A., Zhang, X., Fantin, A., Zhuang, Z., Rivera-Molina, F., Speichinger, K., Prahst, C., Zhang, J., Wang, Y., Davis, G. et al. (2013). The neuropilin 1 cytoplasmic domain is required for VEGF-A-dependent arteriogenesis. *Dev. Cell* **25**, 156-168. doi:10.1016/j.devcel.2013.03.019

Lee, H. S., Cheerathodi, M., Chaki, S. P., Reyes, S. B., Zheng, Y., Lu, Z., Paidassi, H., DerMardirossian, C., Lacy-Hulbert, A., Rivera, G. M. et al. (2015). Protein tyrosine phosphatase-PEST and beta8 integrin regulate spatiotemporal patterns of RhoGDI1 activation in migrating cells. *Mol. Cell. Biol.* **35**, 1401-1413. doi:10.1128/MCB.00112-15

Liebner, S., Corada, M., Bangsow, T., Babbage, J., Taddei, A., Czupalla, C. J., Reis, M., Felici, A., Wolburg, H., Fruttiger, M. et al. (2008). Wnt/beta-catenin signaling controls development of the blood-brain barrier. *J. Cell Biol.* **183**, 409-417. doi:10.1083/jcb.200806024

Mao, X., Fujiwara, Y., Chapdelaine, A., Yang, H. and Orkin, S. H. (2001). Activation of EGFP expression by Cre-mediated excision in a new ROSA26 reporter mouse strain. *Blood* **97**, 324-326. doi:10.1182/blood.V97.1.324

Mathew, S., Lu, Z., Palamuttam, R. J., Mernaugh, G., Hadziselimovic, A., Chen, J., Bulus, N., Gewin, L. S., Voehler, M., Meves, A. et al. (2012). beta1 integrin NPXY motifs regulate kidney collecting-duct development and maintenance by induced-fit interactions with cytosolic proteins. *Mol. Cell. Biol.* **32**, 4080-4091. doi:10.1128/MCB.00568-12

McCarty, J. H. (2009). Cell adhesion and signaling networks in brain neurovascular units. *Curr. Opin Hematol.* **16**, 209-214. doi:10.1097/MOH.0b013e32832a07eb

McCarty, J. H. (2020). alphavbeta8 integrin adhesion and signaling pathways in development, physiology and disease. *J. Cell Sci.* **133**, jcs239434. doi:10.1242/jcs.239434

McCarty, J. H., Monahan-Earley, R. A., Brown, L. F., Keller, M., Gerhardt, H., Rubin, K., Shani, M., Dvorak, H. F., Wolburg, H., Bader, B. L. et al. (2002). Defective associations between blood vessels and brain parenchyma lead to cerebral hemorrhage in mice lacking αv integrins. *Mol. Cell. Biol.* **22**, 7667-7677. doi:10.1128/MCB.22.21.7667-7677.2002

McCarty, J. H., Cook, A. A. and Hynes, R. O. (2005a). An interaction between {alpha}v{beta}8 integrin and Band 4.1B via a highly conserved region of the Band 4.1 C-terminal domain. *Proc. Natl. Acad. Sci. USA* **102**, 13479-13483. doi:10.1073/pnas.0506068102

McCarty, J. H., Lacy-Hulbert, A., Charest, A., Bronson, R. T., Crowley, D., Housman, D., Savill, J., Roes, J. and Hynes, R. O. (2005b). Selective ablation of αv integrins in the central nervous system leads to cerebral hemorrhage, seizures, axonal degeneration and premature death. *Development* **132**, 165-176. doi:10.1242/dev.01551

McWhorter, F. Y., Wang, T., Nguyen, P., Chung, T. and Liu, W. F. (2013). Modulation of macrophage phenotype by cell shape. *Proc. Natl. Acad. Sci. USA* **110**, 17253-17258. doi:10.1073/pnas.1308887110

Menezes, M. J., McClenahan, F. K., Leiton, C. V., Aranmolate, A., Shan, X. and Colognato, H. (2014). The extracellular matrix protein laminin α2 regulates the maturation and function of the blood-brain barrier. *J. Neurosci.* **34**, 15260-15280. doi:10.1523/JNEUROSCI.3678-13.2014

Mobley, A. K. and McCarty, J. H. (2011). β8 integrin is essential for neuroblast migration in the rostral migratory stream. *Glia* **59**, 1579-1587. doi:10.1002/glia.21199

Mobley, A. K., Tchaicha, J. H., Shin, J., Hossain, M. G. and McCarty, J. H. (2009). Beta8 integrin regulates neurogenesis and neurovascular homeostasis in the adult brain. *J. Cell Sci.* **122**, 1842-1851. doi:10.1242/jcs.043257

Mu, D., Cambier, S., Fjellbirkeland, L., Baron, J. L., Munger, J. S., Kawakatsu, H., Sheppard, D., Broaddus, V. C. and Nishimura, S. L. (2002). The integrin alpha(v)beta8 mediates epithelial homeostasis through MT1-MMP-dependent activation of TGF-β1. *J. Cell Biol.* **157**, 493-507. doi:10.1083/jcb.200109100

Nguyen, H.-L., Lee, Y. J., Shin, J., Lee, E., Park, S. O., McCarty, J. H. and Oh, S. P. (2011). TGF-β signaling in endothelial cells, but not neuroepithelial cells,

is essential for cerebral vascular development. *Lab. Invest.* **91**, 1554-1563. doi:10. 1038/labinvest.2011.124

Nishizuka, S. S. and Mills, G. B. (2016). New era of integrated cancer biomarker discovery using reverse-phase protein arrays. *Drug Metab. Pharmacokinet* **31**, 35-45. doi:10.1016/j.dmpk.2015.11.009

Paredes, I., Himmels, P. and Ruiz de Almodóvar, C. (2018). Neurovascular communication during CNS development. *Dev. Cell* **45**, 10-32. doi:10.1016/j. devcel.2018.01.023

Proctor, J. M., Zang, K., Wang, D., Wang, R. and Reichardt, L. F. (2005). Vascular development of the brain requires β8 integrin expression in the neuroepithelium. *J. Neurosci.* **25**, 9940-9948. doi:10.1523/JNEUROSCI.3467-05.2005

Qin, Y., Garrison, B. S., Ma, W., Wang, R., Jiang, A., Li, J., Mistry, M., Bronson, R. T., Santoro, D., Franco, C. et al. (2018). A milieu molecule for TGF-β required for microglia function in the nervous system. *Cell* **174**, 156-171.e16. doi:10.1016/j.cell.2018.05.027

Reyes, S. B., Narayanan, A. S., Lee, H. S., Tchaicha, J. H., Aldape, K. D., Lang, F. F., Tolias, K. F. and McCarty, J. H. (2013). alphavbeta8 integrin interacts with RhoGDI1 to regulate Rac1 and Cdc42 activation and drive glioblastoma cell invasion. *Mol. Biol. Cell* **24**, 474-482. doi:10.1091/mbc.e12-07-0521

Robinson, M. D., McCarthy, D. J. and Smyth, G. K. (2010). edgeR: a Bioconductor package for differential expression analysis of digital gene expression data. *Bioinformatics* **26**, 139-140. doi:10.1093/bioinformatics/btp616

Rueden, C. T., Schindelin, J., Hiner, M. C., DeZonia, B. E., Walter, A. E., Arena, E. T. and Eliceiri, K. W. (2017). ImageJ2: ImageJ for the next generation of scientific image data. *BMC Bioinformatics* **18**, 529. doi:10.1186/s12859-017-1934-z

Schindelin, J., Arganda-Carreras, I., Frise, E., Kaynig, V., Longair, M., Pietzsch, T., Preibisch, S., Rueden, C., Saalfeld, S., Schmid, B. et al. (2012). Fiji: an open-source platform for biological-image analysis. *Nat. Methods* **9**, 676-682. doi:10.1038/nmeth.2019

Schneider, C. A., Rasband, W. S. and Eliceiri, K. W. (2012). NIH Image to ImageJ: 25 years of image analysis. *Nat. Methods* **9**, 671-675. doi:10.1038/nmeth.2089

Shi, M., Zhu, J., Wang, R., Chen, X., Mi, L., Walz, T. and Springer, T. A. (2011). Latent TGF-beta structure and activation. *Nature* **474**, 343-349. doi:10.1038/nature10152

Simms, V., Bicknell, R. and Heath, V. L. (2017). Development of an ImageJ-based method for analysing the developing zebrafish vasculature. *Vascular Cell* **9**, 2. doi:10.24238/13221-9-1-172

Stenman, J. M., Rajagopal, J., Carroll, T. J., Ishibashi, M., McMahon, J. and McMahon, A. P. (2008). Canonical Wnt signaling regulates organ-specific assembly and differentiation of CNS vasculature. *Science* **322**, 1247-1250. doi:10.1126/science.1164594

Tchaicha, J. H., Mobley, A. K., Hossain, M. G., Aldape, K. D. and McCarty, J. H. (2010). A mosaic mouse model of astrocytoma identifies alphavbeta8 integrin as a negative regulator of tumor angiogenesis. *Oncogene* **29**, 4460-4472. doi:10.1038/onc.2010.199

Tian, Y. C. and Phillips, A. O. (2002). Interaction between the transforming growth factor-beta type II receptor/Smad pathway and beta-catenin during transforming growth factor-beta1-mediated adherens junction disassembly. *Am. J. Pathol.* **160**, 1619-1628. doi:10.1016/S0002-9440(10)61109-1

Tiwary, S., Morales, J. E., Kwiatkowski, S. C., Lang, F. F., Rao, G. and McCarty, J. H. (2018). Metastatic brain tumors disrupt the blood-brain barrier and alter lipid metabolism by inhibiting expression of the endothelial cell fatty acid transporter Mfsd2a. *Sci. Rep.* **8**, 8267. doi:10.1038/s41598-018-26636-6

Toutounchian, J. J. and McCarty, J. H. (2017). Selective expression of eGFP in mouse perivascular astrocytes by modification of the Mlc1 gene using T2A-based ribosome skipping. *Genesis* **55**, e23071. doi:10.1002/dvg.23071

Tronche, F., Kellendonk, C., Kretz, O., Gass, P., Anlag, K., Orban, P. C., Bock, R., Klein, R. and Schütz, G. (1999). Disruption of the glucocorticoid receptor gene in the nervous system results in reduced anxiety. *Nat. Genet.* **23**, 99-103. doi:10.1038/12703

Vallon, M., Yuki, K., Nguyen, T. D., Chang, J., Yuan, J., Siepe, D., Miao, Y., Essler, M., Noda, M., Garcia, K. C. et al. (2018). A RECK-WNT7 receptor-ligand interaction enables isoform-specific regulation of Wnt Bioavailability. *Cell Rep.* **25**, 339-349.e39. doi:10.1016/j.celrep.2018.09.045

Vanlandewijck, M., He, L., Mäe, M. A., Andrae, J., Ando, K., Del Gaudio, F., Nahar, K., Lebouvier, T., Laviña, B., Gouveia, L. et al. (2018). A molecular atlas of cell types and zonation in the brain vasculature. *Nature* **554**, 475-480. doi:10.1038/nature25739

Verkhratsky, A. and Nedergaard, M. (2018). Physiology of Astroglia. *Physiol. Rev.* **98**, 239-389. doi:10.1152/physrev.00042.2016

Wang, J., Dong, X., Zhao, B., Li, J., Lu, C. and Springer, T. A. (2017). Atypical interactions of integrin alphaVbeta8 with pro-TGF-beta1. *Proc. Natl. Acad. Sci. USA* **114**, E4168-E4174. doi:10.1073/pnas.1705129114

Wang, Y., Cho, C., Williams, J., Smallwood, P. M., Zhang, C., Junge, H. J. and Nathans, J. (2018). Interplay of the Norrin and Wnt7a/Wnt7b signaling systems in blood-brain barrier and blood-retina barrier development and maintenance. *Proc. Natl. Acad. Sci. USA* **115**, E11827-E11836. doi:10.1073/pnas.1813217115

Wang, Z., Liu, C.-H., Huang, S., Fu, Z., Tomita, Y., Britton, W. R., Cho, S. S., Chen, C. T., Sun, Y., Ma, J.-X. et al. (2020). Wnt signaling activates MFSD2A to suppress vascular endothelial transcytosis and maintain blood-retinal barrier. *Sci. Adv.* **6**, eaba7457. doi:10.1126/sciadv.aba7457

Worthington, J. J., Klementowicz, J. E. and Travis, M. A. (2011). TGFβ: a sleeping giant awoken by integrins. *Trends Biochem. Sci.* **36**, 47-54. doi:10.1016/j.tibs.2010.08.002

Yang, J., Ma, Y.-Q., Page, R. C., Misra, S., Plow, E. F. and Qin, J. (2009). Structure of an integrin alphaIIb beta3 transmembrane-cytoplasmic heterocomplex provides insight into integrin activation. *Proc. Natl. Acad. Sci. USA* **106**, 17729-17734. doi:10.1073/pnas.0909589106

Zarkada, G., Howard, J. P., Xiao, X., Park, H., Bizou, M., Leclerc, S., Künzel, S. E., Boisseau, B., Li, J., Cagnone, G. et al. (2021). Specialized endothelial tip cells guide neuroretina vascularization and blood-retina-barrier formation. *Dev. Cell* **56**, 2237-2251.e6. doi:10.1016/j.devcel.2021.06.021

Zhang, M., Wang, M., Tan, X., Li, T.-F., Zhang, Y. E. and Chen, D. (2010). Smad3 prevents β-catenin degradation and facilitates β-catenin nuclear translocation in chondrocytes. *J. Biol. Chem.* **285**, 8703-8710. doi:10.1074/jbc.M109.093526

Zhu, J., Motejlek, K., Wang, D., Zang, K., Schmidt, A. and Reichardt, L. F. (2002). β8 integrins are required for vascular morphogenesis in mouse embryos. *Development* **129**, 2891-2903. doi:10.1242/dev.129.12.2891

DEVELOPMENT